Published in final edited form as:
Biomaterials. 2008 October ; 29(29): 4012–4021. doi:10.1016/j.biomaterials.2008.07.004.

Magnetic Nanoparticles with Dual Functional Properties: Drug Delivery and Magnetic Resonance Imaging

Tapan K. Jain[1], **John Richey**[2], **Michelle Strand**[3], **Diandra L. Leslie-Pelecky**[3,+], **Chris Flask**[2], and **Vinod Labhasetwar**[1,4*]

1*Department of Biomedical Engineering, Lerner Research Institute, Cleveland Clinic, Cleveland, OH 44195, USA*

2*Department of Radiology, Case Center for Imaging Research, Case Western Reserve University, Cleveland, OH 44106, USA*

3*Department of Physics & Astronomy and Nebraska Center for Materials and Nanoscience, University of Nebraska-Lincoln, Lincoln, NE 68588-0111, USA*

4*Taussig Cancer Center, Cleveland Clinic, Cleveland, OH 44195, USA*

Abstract

There is significant interest in recent years in developing MNPs having multifunctional characteristics with complimentary roles. In this study, we investigated the drug delivery and magnetic resonance imaging (MRI) properties of our novel oleic acid-coated iron-oxide and pluronic-stabilized magnetic nanoparticles (MNPs). The drug incorporation efficiency of doxorubicin and paclitaxel (alone or in combination) in MNPs was 74–95%; the drug release was sustained and the incorporated drugs had marginal effects on physical (size and zeta potential) or magnetization properties of the MNPs. The drugs in combination incorporated in MNPs demonstrated highly synergistic antiproliferative activity in breast cancer cells. The T_2 relaxivity (r_2) was higher for our MNPs than Feridex IV, whereas the T_1 relaxivity (r_1) was better for Feridex IV than for our MNPs, suggesting greater sensitivity of our MNPs than Feridex IV in T_2 weighted imaging. The circulation half-life ($t_{1/2}$), determined from the changes in the MRI signal intensity in carotid arteries in mice, was longer for our MNPs than Feridex IV ($t_{1/2}$ = 31.2 vs 6.4 min). MNPs with combined characteristics of MRI and drug delivery could be of high clinical significance in the treatment of various disease conditions.

Keywords

Iron-oxide; anticancer agents; imaging; anti-proliferative effects; tumor

1. Introduction

Magnetic nanoparticles (MNPs) have been explored for various biomedical applications that include their use in cell labeling/cell separation [1,2], magnetofection to facilitate gene delivery

*Author for correspondence: Vinod Labhasetwar, Ph.D., Department of Biomedical Engineering/ND20, Cleveland Clinic, 9500 Euclid Avenue, Cleveland, OH 44195, Tel: 216/445-9364, Fax 216/444-9198, E-mail: labhasv@ccf.org.
+Affiliation from May 1, 2008; Department of Physics, University of Texas at Dallas, Richardson, TX 75080, USA

[3], as contrast agents for magnetic resonance imaging (MRI) [4], to induce local hyperthermia in response to an external alternating magnetic field to selectively destroy cancer cells [5], and as a magnetically targeted carrier system in drug delivery applications [6,7]. However, there is significant interest in recent years in developing MNPs having multifunctional characteristics with complimentary roles [8]. For example, the imaging enhancement property of MNPs can be used in conjunction with drug delivery applications for real-time monitoring of drug distribution to the target tissue, as well as to follow the effect of therapeutics on the progression of disease [9].

Nanocarrier drug delivery systems such as polymeric nanoparticles, liposomes, micelles, etc., do not have the inherent imaging characteristics to monitor their distribution *in vivo*. Pharmacokinetic modeling that is commonly used to determine drug distribution in various body compartments (e.g., one compartment model, two compartment model, etc.), based on serum/urine drug levels, is useful for drugs that are administered intravenously without a nanocarrier system where the drug distribution to various tissues is primarily controlled by its diffusion coefficients [10]. Since nanocarriers have a different set of parameters that control their biodistribution, such as their interactions with the components of the reticuloendothelial system (RES) [11], the above pharmacokinetic model cannot predict drug concentration in various body compartments. Further, other factors such as size, shape, surface properties (charge, hydrophilicity/hydrophobicity, etc.) [12], targeting ligand and vascular porosity influence biodistribution of nanocarriers [13]. To develop an optimal therapy, there is a need of a drug carrier system, the biodistribution of which, and hence indirectly that of the associated drugs, can be monitored in real time. This is particularly important in cancer therapy as subtherapeutic dosing not only can pose the risk of tumor relapse but also it could develop drug resistance [14].

Superparamagnetic iron-oxide (SPIO) nanoparticles and ultrasmall superparamagnetic iron - oxide (USPIO) nanoparticles have been widely used for MRI in clinical practice for diagnostic applications (e.g., Feridex IV™ and Endorem™); however, their use as a drug carrier system is still under investigation. The currently used MNPs are primarily dextran-coated iron-oxide particles; the coating is necessary to form a water-dispersible system [15,16]. Although several magnetic materials are under investigation, iron-oxide is the most commonly used magnetic material because of its biodegradable nature, biocompatibility, and its superparamagnetic effects on MRI contrast [17]. Several attempts have been made to use MNPs for drug delivery while retaining their inherent magnetic and imaging properties. In the most commonly used approach, the drug of interest is conjugated to the coated dextran or other polymeric coatings such as starch, polyethylene glycol, block-co-polymers, etc. [6,18]. This approach requires developing complex conjugation chemistry; which often results in limited drug association with MNPs and its quite rapid dissociation [6]. Further the associated drug can also alter the physical and/or surface characteristics of the original MNPs (e.g., hydrodynamic size, charge, stability and magnetization) [19,20] that could influence the biodistribution of MNPs [21] and thus imaging characteristics. In another approach, MNPs are dispersed in polymers (e.g., polylactide and poly dl-lactide *co*-glycolide) that are typically used in developing nanocarriers for drug delivery applications [22]. However, this approach usually results in the formation of large size microparticles with limited encapsulation of MNPs. Hence, the carrier is system has overall magnetization [23–26] that could adversely influence both their drug targeting efficiency in response to an external magnetic field as well as imaging properties. Liposomes or emulsions incorporating both the drug of interest, as well as iron-oxide particles and other contrast agents, have been tested in animal models of cancer for drug delivery and imaging [27,28]; however, the drug loading efficiency of these formulations is usually low (2–3%) [29].

We have recently developed a formulation of MNPs in which the iron-oxide core is first coated with oleic acid (OA) and then OA-coated particles are stabilized with pluronic to form a water-dispersible system [30]. In the present study, we have further investigated the ability of the above formulation for drug delivery and MRI applications. We are specifically interested in evaluating our MNPs for anticancer drug therapy; hence, we selected doxorubicin (DOX) and paclitaxel (PTX) for the combination study. These drugs work by different mechanisms; DOX via intercalating with DNA [31] whereas PTX acts by interacting with microtubules [32,33]. The objectives of the current study were to demonstrate that: i) a single drug or combination of drugs can be incorporated in our MNPs with high efficiency; ii) the combination of drugs in MNPs demonstrate synergistic antiproliferative activity in cancer cells; and iii) the incorporated drugs do not adversely influence the magnetic and imaging properties of the formulation. Further, we determined the circulation half-life of MNPs by measuring the change in the MRI signal intensity in mice carotid arteries.

2. Materials and methods

2.1 Materials

Pluronic F-127 was received as a gift from BASF Corporation (Mt. Olive, NJ). Mohr's salt, 1,10 phenanthroline, hydroxylamine hydrochloride and absolute ethanol (HPLC grade) were obtained from Sigma-Aldrich (St. Louis, MO). Iron (III) chloride hexahydrate ($FeCl_3 \cdot 6H_2O$) 99% pure granulated (Fe(III)), Iron (II) chloride tetrahydrate ($FeCl_2 \cdot 4H_2O$) 99+% (Fe(II)), ammonium hydroxide (5M), oleic acid (OA), concentrated hydrochloric acid (HCl) and liquid scintillation counter cocktail (Scinti Verse I) were purchased from Fisher Scientific (Pittsburgh, PA). Paclitaxel (PTX) was procured from Shanghai 21CEC Pharmaceuticals (China). Doxorubicin hydrochloride (DOX.HCl) was a kind gift received from Dabur Research Foundation (Ghaziabad, India). Feridex IV was obtained from Berlex Laboratories (Montville, NJ). De-ionized water freshly purged with nitrogen gas was used in all the steps involved in the synthesis and formulation of MNPs.

2.2 Synthesis of magnetic nanoparticles

Iron-oxide nanoparticles were prepared by co-precipitation of Fe(III) and Fe(II) with ammonium hydroxide. Typically, 0.1M Fe(III) (30 mL) and 0.1M Fe(II) (15 mL) were mixed, to which 3 mL of 5M ammonium hydroxide solution was added drop-wise over 1 min while stirring on a magnetic stir plate. The mixture was stirred for 20 min under a nitrogen-gas atmosphere to which 100 mg OA was added; the mixture was then heated to 80 °C for 30 min while stirring and then cooled to room temperature. The OA-coated iron-oxide nanoparticles were separated by placing a magnet (12,200 G, Edmund Scientific, Tonawanda, NY) below the beaker for about 5 min and the supernatant was discarded. The coated nanoparticles were washed three times with water and then dispersed in 45 mL of water to which 100 mg of pluronic F-127 was added. The mixture was stirred overnight on a magnetic stir plate; the suspension of MNPs was then centrifuged (Sorvall Legend RT Centrifuge, Thermo Electron Corporation, Waltham, MA) at 1,000 rpm for 15 min at 10 °C to remove large aggregates. The ratio of OA to pluronic was optimized in our previous studies to obtain unaggregated MNPs with low polydispersity [30]. Iron concentration in the formulation was determined using 1,10 phenanthroline colorimetric method and a standard plot prepared using Mohr's salt in the range of 0.5–6.0 μg Fe/mL [34].

2.3 Particle size and zeta potential measurements

The mean hydrodynamic particle size of the MNPs was determined in water by dynamic laser light scattering (DLS) at scattering angle of 90° at 25 °C using NICOMP™ 380 ZLS (Particle Sizing Systems, Santa Barbara, CA). The suspension of MNPs prepared either in water or PBS

buffer (154 mM, pH 7.4) was used to measure zeta potential in phase analysis mode and the current mode at a scattering angle of −14°.

Transmission electron microcopy (TEM) was used to determine the size of the iron-oxide core d using a Philips 201 transmission electron microscope (Philips/FEI Inc., Briarcliff Manor, NY). A drop of dilute aqueous suspension of MNPs was placed onto a Formvar coated 150 mesh copper TEM grid (Ted Pella Inc., Redding, CA) and then air dried. The TEM images were analyzed for size of iron-oxide core using NIH ImageJ software (http://rsb.info.nih.gov/ij/) [35]. The size distribution was determined using the diameters of 50–80 particles in a TEM image.

2.4 Drug loading in magnetic nanoparticles

Doxorubicin hydrochloride (DOX.HCl) was first converted to water-insoluble base (DOX) using the procedure described previously [36]. Ethanolic solutions of either DOX (600 μL, 5mg/mL) or PTX (600 μL, 5mg/mL) or a combination of DOX/PTX 1:1 w/w (300 μl of each drug stock solution, 5 mg/mL) were added drop-wise while stirring to an aqueous dispersion of MNPs (30 mg of particles in 7 mL of water). The mixture was stirred overnight (~16 h) to allow partitioning of drug(s) into the OA layer surrounding the iron-oxide core. Drug-loaded MNPs were separated from the free drug using a magnet. Typically, a glass vial (8 mL glass vial, 17 mm diameter, Fisher Scientific) containing drug-loaded MNPs was placed between two magnets (opposite poles facing each other) and allowed to stand for ~ 5 h to separate MNPs under the magnetic field. The magnets were placed just below the top meniscus of MNPs suspension so that if there are any insoluble unloaded drug particles (because of the limited solubility of drugs in water), they would settle down and only MNPs loaded with drug(s) would be attracted towards the magnets. The liquid was removed carefully without disturbing the MNPs attracted toward the magnets. The drug-loaded MNPs were washed twice by re-suspending them in water and separating by using magnets as above. Each washing was analyzed for drug concentration to ensure the free drug that had not been partitioned in the OA layer was removed. Finally, the drug-loaded MNPs were dispersed in 5 mL of sterile, distilled water.

To determine DOX loading, a 200 μL aliquot of the suspension of MNPs was lyophilized for 2 days (at −50 °C and 7 μm Hg vacuum, Freezone 4.5, LABCONCO, Kansas City, MO) and the weight of each lyophilized sample was measured from the difference in the weight of the tube without the sample and after lyophilization. To each lyophilized sample, 2 mL of 12.5% v/v methanolic solution in chloroform was added to extract the drug. The samples were kept on a shaker rotating at 100 rpm at room temperature for 24 h (Environ Shaker, Model 3527, Lab-Line Instruments, Melrose Park, IL); and then centrifuged for 10 min at 14,000 × g at 4 °C using an Eppendorf microcentrifuge (5417R, Eppendorf-Netheler–Hinz-GmbH, Hamburg, Germany). A 100 μL aliquot of supernatant from each sample was diluted to 2 mL with 12.5% v/v methanol in chloroform mixture (the base form of this drug is soluble in this combination of solvents) to determine DOX concentration using a fluorescence spectrophotometer (LS55 Fluorescence Spectrophotometer, PerkinElmer LLC, Shelton, CT) at λ_{ex} = 485 nm and λ_{em} = 591 nm.

To determine PTX loading, tritium-labeled PTX (Moravek Biochemicals, Brea, CA) was used for loading. In a typical procedure, 5 μCi of ^{3}H-PTX were mixed with 4 mg of unlabeled PTX in 800 μL of ethanol, out of which 600 μL was used for drug loading in MNPs as described above and the remaining solution was used to prepare a standard plot. To determine drug loading, a 200 μL aliquot of PTX-loaded MNPs was lyophilized as above to which 1 mL of absolute ethanol was added and the sample was incubated for 24 h. The particles were centrifuged at 14,000 × g for 10 min at 4 °C. To 300 μL of the supernatant, 4 mL of liquid scintillation counter cocktail was added and radioactivity was measured using a scintillation

counter (Beckman LS 6500, Beckman instruments Inc. Fullerton CA). A standard plot was prepared in the drug concentration range of 1 – 50 μg/mL using the identical procedure.

2.5 Antiproliferative activity of drug loaded magnetic nanoparticles

MCF-7 (breast cancer) cells procured from American Type Culture Collection (ATCC, Manassas, VA) were maintained in RPMI 1640 medium supplemented with 10% fetal bovine serum and 100 μg/mL penicillin G and 100 μg/mL streptomycin (Gibco BRL, Grand Island, NY) in an incubator (Thermo Electron Corporation, Asheville, NC) at 37 °C in a humidified and 5% CO_2 atmosphere. Cells were seeded at 3,000 cells per well in 96-well plates and were allowed to attach for 24 h. Cells were treated either with drugs in solution or drugs incorporated in MNPs at different doses to determine IC_{50} values.

Different dilution of drugs were prepared in culture medium using stock solutions of PTX (4.8 mg/mL) in 200 proof ethanol and DOX.HCl (3.8 mg/mL) in 77% ethanol Similarly, a stock suspension of drug-loaded MNPs was diluted appropriately in culture medium to provide an equivalent amount of drugs used in solution. Medium from wells was replaced with either the suspension of drug-loaded MNPs or drug in solution prepared in culture medium as above. Cells were incubated as above; the medium was changed at 2 and 4 days after the treatment and no further drugs were added. Medium and control MNPs (without drug) were the respective controls for drug in solution and drug-loaded MNPs. Cell viability was determined on day 5 using an MTS assay (CellTiter 96 AQueous, Promega, Madison, WI). IC_{50} values were calculated using the following equation:

$$y=\frac{A_1 - A_2}{1+(x/x_0)^p}+A_2$$

where x is drug concentration added, y is % growth determined by MTS assay, A_1 corresponds to % growth on the top plateau region of the curve, A_2 corresponds to % growth on the bottom plateau region of the curve; x_0 corresponds to the inflexion point of the curve and p corresponds to the slope. Experimental data points were fit to this equation using Origin 7.5 (OriginLab Corporation, Northampton, MA) and IC_{50} was determined by putting $y = 50$ in the above equation and calculating x using the parameters obtained after curve fitting.

2.6 Preparation of phantom agar gels for imaging

Suspensions of MNPs in the concentration range of 0–50 μg/mL of iron were prepared in PBS. A 2.5% w/v agar solution was prepared by heating 250 mg of agar in 10 mL of PBS at 80°C for 20 min. For preparing phantom gels, 160 μL of the above agar solution was mixed with 840 μL of MNP suspension at each concentration, and was preheated to 60 °C to prevent gelation while mixing. MNPs and agar gel were mixed thoroughly while warm, in 1.5 mL microcentrifuge tubes, by turning the tubes upside down repeatedly. An aliquot of 250 μL of this mixture was transferred quickly to a 300 μL microcentrifuge tube and then allowed to cool to room temperature.

2.7 Magnetization measurements

MRI contrast agents work by changing the relaxivity (T_1 and T_2) of hydrogen nuclei in their vicinity due to the additional magnetic field they produce. The static magnetic properties of phantom gels were measured at room temperature using a MicroMag 2900 alternating gradient field magnetometer (AGFM, Princeton Measurements Corp, Princeton, NJ). Small amounts of the gels were transferred to polyethylene bags and sealed. Magnetization as a function of field *M(H)* was measured with a maximum field of 1.2 T. The saturation magnetization M_S and number of effective Bohr magnetons per MNP were determined by fitting the magnetization curve to a Langevin function plus a diamagnetic contribution (χ) due to the gel and the polyethylene bag.

2.8 Measurements of imaging characteristics of magnetic nanoparticles in phantom gels

Tubes containing MNPs in gel were positioned near the isocenter in a Bruker Biospec 9.4T MRI scanner (Bruker BioSpin Corporation, Billerica, MA) within a 72 mm transmit/receive coil with a homogeneous B_1 field to obtain the MRI images. The host software (Paravision ver 3.0.2) was used for data acquisition, reconstruction and visualization/analysis of the images. To estimate the transverse relaxation time (T_2) for each sample, coronal images (TH=2mm) were acquired at various echo times (TE) from 10 ms to 340 ms with a repetition time (TR) of 10,000 ms. Similarly, the T_1 relaxation time for each sample was measured by varying TR between 15.4 ms to 10,000 ms while keeping TE constant at 10 ms. After acquiring the images, the magnitude image intensities were measured within manually-drawn regions of interest (ROIs) for each of the samples. Relaxation rates R_1 ($R_1=1/T_1$) and R_2 ($R_2=1/T_2$) were calculated by mono-exponential curve fitting of the signal intensity vs. time (TE or TR) data (using Origin 7.5 software). The following equations were used for curve fitting:

For relaxation rate R_1: $y = A*[1 - \exp(-R_1*TR)]$

For relaxation rate R_2 : $y = A + C*[\exp(-R_2*TE)]$

R_1 or R_2 was calculated for gels with different iron concentration. T_1 relaxivity, r_1 (or T_2 relaxivity, r_2) was then calculated as slope from a plot of R_1 (or R_2) vs. iron concentration in gels to compare different formulations for sensitivity of the contrast enhancing properties.

2.9 Clarence of magnetic nanoparticles in vivo

Athymic nude mice (male, nu/nu, 30–40 g Charles River, Wilmington, MA) were maintained on isoflurane anesthesia throughout the experiment. A suspension of MNPs or Feridex IV (7 mg Fe/kg) diluted in mannitol-citrate isotonic solution was injected via tail vein over 40 sec using a 30 gauge needle connected to a PE20 tubing. The tubing was flushed with heparinized saline prior to nanoparticle injection. Dynamic scanning of mice was performed using a 9.4T Bruker Biospec MRI to observe the changes in the signal intensity in both the carotid arteries. A FLASH sequence (TR/TE = 12.4/3.5 ms, FOV = 2.0 × 2 .0 cm, matrix = 128 × 128, alpha = 30°, Slice thickness = 1 mm) was used to acquire axial images of the carotid arteries for each animal. Typically, the pre-injection dynamic scans were performed for the first 4 images and then nanoparticles were injected at the end of the 4^{th} acquisition of the dynamic scan image. The Regions of Interest (ROIs) were drawn in for both the carotid arteries for the each acquired image. The signal intensities within ROIs were measured at different time intervals. Relative concentration of iron-oxide nanoparticles (MNPs or Feridex IV) was estimated from the signal intensity changes using the following equation which has been used previously by others [37]:

$$[\mathrm{MNP}] \propto -\ln\left[\frac{S(t)}{S_o}\right]$$

where, S_o is the signal intensity before injection and S(t) is the signal intensity at time “t” post injection of contrast agent and TE, echo time was kept same for all the acquisitions. This equation is merely a simplification of the Bloch equations for the FLASH acquisitions with short TR and T2* changes caused by the MNP contrast agent.

3.0 Statistical Analysis

All of the results are expressed as mean ± s.e.m. Origin 7.5 was used to fit dose-response and exponential equations to calculate IC_{50} values and relaxation times (T_1 and T_2), respectively.

3. Results

3.1 Physical characterization of magnetic nanoparticles

The mean hydrodynamic diameter of our MNPs with and without incorporated drugs (measured in distilled water or in PBS) was in the range of 210–250 nm. The incorporated drugs had an insignificant effect on the mean hydrodynamic size. The mean hydrodynamic diameter of Feridex IV was ~140 nm, either in water or PBS, which is lower than the mean diameter of our MNPs (Table 1). However, the polydispersity index of our MNPs was significantly lower compared to that of Feridex IV. Loading of PTX did not change the zeta potential of MNPs but DOX loading reduced the negative zeta potential of MNPs (Table 1). All the formulations showed negative zeta potential in water but slightly positive zeta potential in PBS. TEM of our MNPs showed a core particle size of 10–25 nm (Fig 1a). None of the MNP formulations showed measurable coercivity. At the highest concentration, the drug-loaded MNPs have noticeably lower saturation magnetizations per weight or volume than the unloaded MNPs (Table 2). The saturation magnetization of our MNPs, with or without drugs, was higher than that of Feridex IV at each of the iron concentrations studied.

3.2 Drug loading and release behavior of paclitaxel from magnetic nanoparticles

The drug entrapment efficiency for PTX was slightly higher than that for DOX (95% vs. 82%). The total entrapment efficiency was 85% when the two drugs were used in combination, with about 74% for DOX and 96% for PTX (Table 3). PTX release was sustained; with about 25% cumulative release occurring in 48 h, 60% in one week, and almost complete release over three weeks (Fig 1b). The release profile was PTX was almost identical to that reported for the DOX-loaded MNPs in our previous study [30].

3.3 Antiproliferative effect of the drug loaded magnetic nanoparticles

Drug-loaded MNPs or drugs in solution exhibited the typical sigmoidal dose-dependent antiproliferative effect on MCF-7 cells (Fig 2). PTX-loaded in MNPs and PTX in solution showed almost similar IC_{50} values (10.6 ng/mL vs. 9.8 ng/mL); however, DOX-loaded in MNPs and DOX in solution showed a significant difference in the IC_{50} values (796 ng/mL vs. 103 ng/mL) (Fig 3a). In the case of combination treatment (PTX:DOX ratio = 1:1 w/w), the drugs loaded in MNPs showed slightly higher IC_{50} values than the combination in solution (15.5 ng/mL vs. 3.4 ng/mL).

The combination index (CI) values were used to determine whether the effect with drug combination is synergistic, additive or antagonistic. *Calcusyn v.2* (Biosoft, Ferguson, MO) was used for calculating the CI values, which are based on the Median Effect of each drug as described by Chou and Talalay [38]. CI values <1, =1 and >1 are considered synergistic, additive, and antagonistic effects, respectively. The combination treatment showed a highly synergistic effect in the concentration range of 0.5 –100 ng/mL but the effect was antagonistic at lower (0.001–0.5 ng/mL) and higher (500–20,000 ng/mL) drug concentration ranges (Fig 3b). The effect was consistent when the drugs were used in combination in solution or loaded in MNPs. Cells treated with an equivalent amount of control MNPs (without drug) did not show any cytotoxicity, as the cell growth was almost identical as in the medium control.

3.4 Magnetic resonance imaging characteristics of magnetic nanoparticles

The transverse relaxation time T_2 of water was reduced significantly by MNPs relative to the control gel. As the MNP concentration, measured in μg Fe/mL, was increased in the phantom gels, the signal intensity decreased and the relaxation curves became steeper (Fig 4a & 4b). As the particle concentration increased from 0.5 μg Fe/mL to 50 μg Fe/mL, the T_2 relaxation times were reduced from 110 ms to 2.9 ms, whereas for Feridex IV, T_2 times were reduced from 123

ms to 4.0 ms. As expected, the relaxation rate, $R_2=1/T_2$, was linearly proportional to the particle concentration (Fig 4c). T_2 relaxivities (r_2) for our MNPs and Feridex were 6.8 $s^{-1}\mu g^{-1}mL$ and 4.8 $s^{-1}\mu g^{-1}mL$, respectively (Fig 5a). Similarly, the relaxation rate, R_1 was found to be proportional to particle concentration (Fig 5b). T_1 relaxivities (r_1) for MNPs and Feridex IV were 3.8×10^{-3} $s^{-1}\mu g^{-1}mL$ and 13.9×10^{-3} $s^{-1}\mu g^{-1}mL$, respectively (Fig 5c).

3.5 Effect of drug loading on imaging properties of magnetic nanoparticles

The T_2 relaxivity (r_2) calculated from the slope of $1/T_2$ vs. Fe concentration plot was found to be in the following order: MNPs (without drug) > PTX-loaded MNPs > Feridex IV > DOX-loaded MNPs, suggesting the influence of the incorporated drugs; however, the T_2 relaxivity values of drug-loaded MNPs (DOX-MNPs, 4.4 $s^{-1}\mu g^{-1}mL$ and PTX-MNPs, 5.3 $s^{-1}\mu g^{-1}mL$) were closer to that for Feridex IV, 4.8 $s^{-1}\mu g^{-1}mL$ (Fig 5a & 5c). T_1 relaxivity (r_1) was in the following order: Feridex IV > MNPs > PTX-loaded MNPs > DOX-loaded MNPs (Fig 5b & 5c). DOX loading reduced the T_1 relaxivity of MNPs whereas PTX loading did not show significant change in the T_1 relaxivity of MNPs (Fig 5b & 5c).

3.6 Clarence of magnetic nanoparticles in vivo

Immediately following injection of Feridex IV or our MNPs, rapid decrease in the MR signal intensity was observed in the carotid arteries. Within the first five minutes, both Feridex IV and our MNPs showed a decrease in signal intensity but thereafter Feridex IV continued to show an exponential increase in the MR signal intensity whereas the intensity with our MNPs remained almost stable for ~30 min prior to rapid increase (Fig 6a). The half-life ($t_{1/2}$) of clearance calculated from the relative concentration vs. time profile for Feridex IV was 6.4 min whereas that for our MNPs was 31.2 min (Fig 6b).

4. Discussion

Developing MNPs with the dual functional properties of drug delivery and imaging is a challenging task as it requires meeting the requirements of both the applications without significantly compromising the efficiency of either one. Our overall results demonstrated that drugs either alone or in combination can be incorporated into the formulation with high efficiency and without significantly influencing the imaging properties. This is due to the unique formulation characteristics of our MNPs, in which hydrophobic drugs partition into the OA layer surrounding the iron-oxide core without significantly affecting the physical (size or surface) properties of the formulation or magnetization characteristics of the iron-oxide core.

Pluronic F-127 is a block copolymer with poly (propylene oxide) as a central unit that is flanked by polyethylene oxide chains on both sides. The hydrophobic segment of poly (propylene oxide) (PPO) chain anchors into the hydrophobic OA coating, extending the hydrophilic, polyethylene oxide (PEO) chains towards the aqueous phase and imparting steric stability and aqueous dispersity to the particles. The coated OA and PEO contribute toward the hydrodynamic diameter of MNPs which is higher than the diameter of the iron-oxide core as determined using TEM to be in the range of 10–25 nm. It appears that the incorporation of DOX slightly reduces the negative zeta potential of MNPs but PTX has no effect. This may be because of the basic nature of DOX, which may have partially neutralized the carboxyl groups of OA coated on iron-oxide core; however it had insignificant effect on the mean hydrodynamic diameter of MNPs. Zeta potentials of all the formulations measured in PBS ranged from close to neutral to slightly positive. This could be because of the counter-ion effect of the salts present in the buffer.

Our results demonstrate that the loading efficiency was slightly higher for PTX than for DOX (95% vs. 82%) which may be because of the difference in their hydrophobicity; PTX being

more hydrophobic than DOX (logP, PTX = 4 vs. DOX= 1.85) [39,40]. In cancer therapy, combination drug therapy is used primarily to achieve a synergistic effect so that the overall total dose of the drugs required is reduced, which is anticipated to result in a better therapeutic outcome with fewer side effects than single-drug therapy. Our results demonstrated that DOX in combination with PTX significantly reduced the IC_{50} value, and demonstrated highly synergistic activity in a specific concentration range. Although the synergistic effect was also seen with drugs in solution, the advantage of using the drug combination in MNPs would be that the same ratio of drugs, as optimized with *in vitro* experiments, can be delivered to the tumor tissue *in vivo*. With drugs in solution, the amount of each drug reaching the target tissue would depend on their pharmacokinetic and pharmacodynamic parameters, and hence would require further optimization of doses. Although we have tested the two drugs in 1:1 w/w ratio to provide a proof of principle that a combination of drugs can be delivered using our MNPs, the dosages can be further optimized.

The release of incorporated drugs from the MNPs extended over three weeks. The initial release could be because of the diffusion of the drug from the OA layer due to the difference in the concentration gradient with the outside environment, but the subsequent release is likely due to the dissociation of the OA layer from the iron-oxide core. The relatively higher IC_{50} values observed with DOX- or the DOX/PTX combination-loaded MNPs relative to drugs in solution could result from the sustained release properties of our MNPs, as only a fraction of the incorporated drug(s) is released over the experimental period of 5 days. However, such a difference in the IC_{50} was not seen when PTX alone was tested in MNPs and in solution. This may be because of the potent nature of PTX relative to DOX, as is evident from their respective IC_{50} values (9.8 ng/L vs. 796 ng/mL). It is interesting to note that the IC_{50} of DOX alone is high, but in combination with PTX, it is significantly reduced. Thus, one can foresee the use of such a combination to reduce the dose of DOX to minimize its cardiotoxicity [41–43].

Achieving sustained drug release in cancer therapy is not only important for anticancer efficacy but also to prevent the cancer from relapsing and developing drug resistance [44,45]. Alexiou *et al.* [6] observed complete dissociation of mitoxantrone within 1 h *in vitro*. Such a formulation could cause premature leaching of the associated drug into the systemic circulation prior to the nanoparticles accumulation in the target tumor tissue. Several mechanisms have been proposed to explain the enhanced efficacy of drugs delivered using MNPs. Wang *et al.* [46] have demonstrated greater cellular accumulation of daunorubucin in resistant K562 leukemia cells which was suggested to be due to nanoparticles competitively binding to the P-glycoprotein, thus preventing the drug efflux. Rudge *et al.* studied the cytotoxicity of magnetically targeted carriers loaded with DOX on SK-Br3 cells and demonstrated dose-dependent antiproliferative effect [47]. Thus there are significant potential advantages of using MNPs for the delivery of anticancer agents.

The T_2 relaxation process occurs because of the exchange of energy between protons in water molecules. In the presence of an externally applied magnetic field, SPIO nanoparticles create inhomogeneity in the magnetic field affecting the microenvironment that results in dephasing of the magnetic moments of protons and hence T_2 shortening. The relatively higher T_2 relaxivity (r_2) of our MNPs relative to Feridex IV suggests a better contrast property of our formulation, and hence can be more sensitive as an MRI contrast agent. This may be attributed to the ability of MNPs to induce more local inhomogeneity in the magnetic field than Feridex IV, as is evident by the high saturation magnetization values of MNP-doped phantom gels (Table 2). At high magnetic fields (like the 9.4 T of our MRI measurements), the local increase in magnetic field is related to the saturation magnetization of the superparamagnetic contrast agent [48]. Greater local magnetic field inhomogeniety creates more contrast and hence greater T_2 relaxivity (r_2).

We also found that T_1 relaxivity in the following order of decreasing values: Feridex IV > MNPs > PTX-loaded MNPs > DOX-loaded MNPs. Since the T_1 relaxation process requires close proximity of the hydrogen atoms to the contrast agent [49], it appears that the dextran coating used in Feridex IV, because of its more hydrophilic nature than pluronic coating, allows closer proximity of the contrast agent to water molecules, leading to shortening of the spin-lattice relaxation time. Pluronics contain hydrophilic PEO and hydrophobic PPO chains, and perhaps the OA coating causes our formulation to be less hydrophilic than dextran-coated Feridex IV, and hence has a reduced hydration effect, thus causing reduced proximity of water molecules to the iron-oxide core of MNPs. The drug loadings in our MNPs seem to further decrease the T_1 relaxivity of MNPs slightly, perhaps because the hydrophobic nature of the drugs further decreases the hydrophilicity of MNPs, even though the incorporated drugs did not change the hydrodynamic size.

One of the key parameters to successfully develop our MNPs for drug delivery and imaging of tumor is minimizing their uptake by circulating macrophages to prevent rapid clearance by the reticuloendothelial system (RES). We anticipated that the pluronic coating of our MNPs would impart that characteristic [50–52]. Relatively slow clearance of our MNPs than Feridex IV supports the role of pluronic coating. The initial rapid increase in signal intensity could be due to biodistribution of injected nanoparticles in the animal vasculature. The clearance of injected nanoparticles also depends on the chain length of PEO. Hence, it would be interesting to determine how different pluronics varying in the ratio of PPO:PEO chain length influence the circulation time of MNPs. Prolonged circulation time would not only allow MNPs to localize drug(s) into the tumor tissue due to leaky vasculature but also to facilitate imaging of the tumor. It is known that tumor-sprouted vessels are greater in both number and diameter than their healthy counterparts [13,53,54]. This abnormal vascularity can be studied and quantified to monitor the effect of chemotherapy on tumor growth. Apart from the drug delivery and imaging applications, our drug-loaded MNPs can be used to enhance the efficacy of drugs for cancer therapy by inducing hyperthermia in response to an alternating magnetic field [5, 55]. Studies have shown that hyperthermia can sensitize cancer cells to the drug effect [56, 57]. Such a strategy can be useful for treating cancers which are refractory to normal chemo- or radiation therapy. The magnetic properties can also be used for magnetic targeting with the assistance of external magnetic field gradients, thus concentrating the drug effects to the target area.

5. Conclusions

Our MNPs can be loaded with water-insoluble anticancer therapeutics with high efficiency either alone or in combination for synergistic activity while retaining their MRI property. Further our MNPs demonstrated prolonged circulation time in mice, an important characteristic for drug delivery and vascular imaging. Thus, our MNPs can be potentially developed with the dual functional properties of drug delivery and imaging, which would have significant clinical applications, particularly in real time monitoring of drug distribution as well as to study the response of chemotherapy on tumor progression.

Acknowledgements

The study reported here is funded by grant R01 EB005822 (to VL) from the National Institute of Biomedical Imaging and Bioengineering of the National Institutes of Health. Authors thank Ms. Melissa Jedlicka for proof reading the manuscript.

References

1. Bulte JW, Douglas T, Witwer B, Zhang SC, Strable E, Lewis BK, et al. Magnetodendrimers allow endosomal magnetic labeling and in vivo tracking of stem cells. Nat Biotechnol 2001;19:1141–1147. [PubMed: 11731783]
2. Olsvik O, Popovic T, Skjerve E, Cudjoe KS, Hornes E, Ugelstad J, et al. Magnetic separation techniques in diagnostic microbiology. Clin Microbiol Rev 1994;7:43–54. [PubMed: 8118790]
3. Scherer F, Anton M, Schillinger U, Henke J, Bergemann C, Kruger A, et al. Magnetofection: enhancing and targeting gene delivery by magnetic force in vitro and in vivo. Gene Ther 2002;9:102–109. [PubMed: 11857068]
4. Wang YX, Hussain SM, Krestin GP. Superparamagnetic iron oxide contrast agents: physicochemical characteristics and applications in MR imaging. Eur Radiol 2001;11:2319–2331. [PubMed: 11702180]
5. Johannsen M, Gneveckow U, Eckelt L, Feussner A, Waldofner N, Scholz R, et al. Clinical hyperthermia of prostate cancer using magnetic nanoparticles: presentation of a new interstitial technique. Int J Hyperthermia 2005;21:637–647. [PubMed: 16304715]
6. Alexiou C, Arnold W, Klein RJ, Parak FG, Hulin P, Bergemann C, et al. Locoregional cancer treatment with magnetic drug targeting. Cancer Res 2000;60:6641–6648. [PubMed: 11118047]
7. Lubbe AS, Bergemann C, Riess H, Schriever F, Reichardt P, Possinger K, et al. Clinical experiences with magnetic drug targeting: a phase I study with 4'-epidoxorubicin in 14 patients with advanced solid tumors. Cancer Res 1996;56:4686–4693. [PubMed: 8840985]
8. Huh YM, Jun YW, Song HT, Kim S, Choi JS, Lee JH, et al. In vivo magnetic resonance detection of cancer by using multifunctional magnetic nanocrystals. J Am Chem Soc 2005;127:12387–12391. [PubMed: 16131220]
9. Medarova Z, Pham W, Kim Y, Dai GP, Moore A. In vivo imaging of tumor response to therapy using a dual-modality imaging strategy. Int J Cancer 2006;118:2796–2802. [PubMed: 16385568]
10. Gibaldi, M. Pharmacokinetics. 2nd ed.. New York, New York: Marcel Dekker Inc; 1982.
11. Owens DE 3rd, Peppas NA. Opsonization, biodistribution, and pharmacokinetics of polymeric nanoparticles. Int J Pharm 2006;307:93–102. [PubMed: 16303268]
12. Stolnik S, Illum L, Davis SS. Long Circulating Microparticulate Drug Carriers. Adv Drug Del Rev 1995;16:195–214.
13. Yuan F, Dellian M, Fukumura D, Leunig M, Berk DA, Torchilin VP, et al. Vascular permeability in a human tumor xenograft: molecular size dependence and cutoff size. Cancer Res 1995;55:3752–3756. [PubMed: 7641188]
14. Vijayaraghavalu S, Raghavan D, Labhasetwar V. Nanoparticles for delivery of chemotherapeutic agents to tumors. Curr Opin Investig Drugs 2007;8:477–484.
15. Bulte JW, Brooks RA, Moskowitz BM, Bryant LH Jr, Frank JA. Relaxometry and magnetometry of the MR contrast agent MION-46L. Magn Reson Med 1999;42:379–384. [PubMed: 10440963]
16. Jung CW, Jacobs P. Physical and chemical properties of superparamagnetic iron oxide MR contrast agents: ferumoxides, ferumoxtran, ferumoxsil. Magn Reson Imaging 1995;13:661–674. [PubMed: 8569441]
17. Okon E, Pouliquen D, Okon P, Kovaleva ZV, Stepanova TP, Lavit SG, et al. Biodegradation of magnetite dextran nanoparticles in the rat. A histologic and biophysical study. Lab Invest 1994;71:895–903. [PubMed: 7807971]
18. Kohler N, Sun C, Fichtenholtz A, Gunn J, Fang C, Zhang M. Methotrexate-immobilized poly(ethylene glycol) magnetic nanoparticles for MR imaging and drug delivery. Small 2006;2:785–792. [PubMed: 17193123]
19. Arias JL, Ruiz MA, Gallardo V, Delgado AV. Tegafur loading and release properties of magnetite/poly(alkylcyanoacrylate) (core/shell) nanoparticles. J Control Release 2008;125:50–58. [PubMed: 17949844]
20. Kim SY, Lee YM. Taxol-loaded block copolymer nanospheres composed of methoxy poly(ethylene glycol) and poly(epsilon-caprolactone) as novel anticancer drug carriers. Biomaterials 2001;22:1697–1704. [PubMed: 11396872]

21. Chouly C, Pouliquen D, Lucet I, Jeune JJ, Jallet P. Development of superparamagnetic nanoparticles for MRI: Effect of particle size, charge and surface nature on biodistribution. J Microencapsul 1996;13:245–255. [PubMed: 8860681]
22. Chattopadhyay P, Gupta RB. Supercritical CO2 based production of magnetically responsive micro- and nanoparticles for drug targeting. Industrial & Engineering Chemistry Research 2002;41:6049–6058.
23. Ramirez LP, Landfester K. Magnetic polystyrene nanoparticles with a high magnetite content obtained by miniemulsion processes. Macromol Chem Phys 2003;204:22–31.
24. Dresco PA, Zaitsev VS, Gambino RJ, Chu B. Preparation and properties of magnetite and polymer magnetite nanoparticles. Langmuir 1999;15:1945–1951.
25. Liu XQ, Novosad V, Rozhkova EA, Chen HT, Yefremenko V, Pearson J, et al. Surface functionalized biocompatible magnetic nanospheres for cancer hyperthermia. Ieee Transactions on Magnetics 2007;43:2462–2464.
26. Hamoudeh M, Al Faraj A, Canet-Soulas E, Bessueille F, Leonard D, Fessi H. Elaboration of PLLA-based superparamagnetic nanoparticles: characterization, magnetic behaviour study and in vitro relaxivity evaluation. Int J Pharm 2007;338:248–257. [PubMed: 17317054]
27. Kubo T, Sugita T, Shimose S, Nitta Y, Ikuta Y, Murakami T. Targeted systemic chemotherapy using magnetic liposomes with incorporated adriamycin for osteosarcoma in hamsters. Int J Oncol 2001;18:121–125. [PubMed: 11115548]
28. Zhang JQ, Zhang ZR, Yang H, Tan QY, Qin SR, Qiu XL. Lyophilized paclitaxel magnetoliposomes as a potential drug delivery system for breast carcinoma via parenteral administration: In vitro and in vivo studies. Pharm Res 2005;22:573–583. [PubMed: 15846465]
29. Dandamudi S, Campbell RB. The drug loading, cytotoxicty and tumor vascular targeting characteristics of magnetite in magnetic drug targeting. Biomaterials 2007;28:4673–4683. [PubMed: 17688940]
30. Jain TK, Morales MA, Sahoo SK, Leslie-Pelecky DL, Labhasetwar V. Iron oxide nanoparticles for sustained delivery of anticancer agents. Mol Pharm 2005;2:194–205. [PubMed: 15934780]
31. D'Arpa P, Liu LF. Topoisomerase-targeting antitumor drugs. Biochim Biophys Acta 1989;989:163–177. [PubMed: 2557085]
32. Schiff PB, Fant J, Horwitz SB. Promotion of microtubule assembly in vitro by taxol. Nature 1979;277:665–667. [PubMed: 423966]
33. Honore S, Pasquier E, Braguer D. Understanding microtubule dynamics for improved cancer therapy. Cell Mol Life Sci 2005;62:3039–3056. [PubMed: 16314924]
34. Jeffery, GH.; Bassett, J.; Mendham, J.; Denny, RC. Vogel's Text Book of Quantitative Chemical Analysis. 5th ed.. New York: John Wiley & Sons Inc; 1989. p. 690-692.
35. Abramoff MD, Magelhaes PJ, Ram SJ. Image Processing with ImageJ. Biophotonics International 2004;11:36–42.
36. Yolles S, Aslund B, Morton JF, Olson OT, Rosenberg B. Timed-released depot for anticancer agents. II. Acta Pharm Suec 1978;15:382–388. [PubMed: 747096]
37. Moffat BA, Reddy GR, McConville P, Hall DE, Chenevert TL, Kopelman RR, et al. A novel polyacrylamide magnetic nanoparticle contrast agent for molecular imaging using MRI. Mol Imaging 2003;2:324–332. [PubMed: 14717331]
38. Chou TC, Talalay P. Analysis of combined drug effects - a new look at a very old problem. Trends Pharmacol Sci 1983;4:450–454.
39. Niethammer A, Gaedicke G, Lode HN, Wrasidlo W. Synthesis and preclinical characterization of a paclitaxel prodrug with improved antitumor activity and water solubility. Bioconjug Chem 2001;12:414–420. [PubMed: 11353540]
40. Hansch, C.; Leo, A. Exploring QSAR. Washington, DC: American Chemical Society; 1995.
41. Gottlieb J, Lefrak E, O'Brien P, Burgess M. Fatal adriamycin cardiomyopathy: Prevention by dose limitation. Proc Am Assoc Cancer Res 1973;14:88.
42. Lefrak EA, Pitha J, Rosenheim S, Gottlieb JA. A clinicopathologic analysis of adriamycin cardiotoxicity. Cancer 1973;32:302–314. [PubMed: 4353012]

43. Rinehart JJ, Lewis RP, Balcerzak SP. Adriamycin cardiotoxicity in man. Ann Intern Med 1974;81:475–478. [PubMed: 4277990]
44. Links M, Brown R. Clinical relevance of the molecular mechanisms of resistance to anti-cancer drugs. Expert Rev Mol Med 1999;1999:1–21. [PubMed: 14585120]
45. Krishna, R.; Mayer, L. Applications of liposome technology to overcome multidrug resistance in solid tumors. In: Gregoriadis, G.; McCormack, B., editors. Targeting of Drugs 6: Strategies for Stealth Therapeutic Systems. New York: NATO ASI Series, Plenum Press; 1998. p. 95-108.
46. Wang XM, Zhang RY, Wu CH, Dai YY, Song M, Gutmann S, et al. The application of Fe3O4 nanoparticles in cancer research: A new strategy to inhibit drug resistance. Journal of Biomedical Materials Research Part A 2007;80A:852–860. [PubMed: 17072850]
47. Rudge SR, Kurtz TL, Vessely CR, Catterall LG, Williamson DL. Preparation, characterization, and performance of magnetic iron-carbon composite microparticles for chemotherapy. Biomaterials 2000;21:1411–1420. [PubMed: 10872770]
48. Westbrook, C.; Roth, CK.; Talbol, J. MRI in Practice. 3rd ed.. Malden, MA: Blackwell Publishing Inc.; 2005.
49. Okuhata Y. Delivery of diagnostic agents for magnetic resonance imaging. Adv Drug Deliv Rev 1999;37:121–137. [PubMed: 10837731]
50. Moghimi SM, Muir IS, Illum L, Davis SS, Kolb-Bachofen V. Coating particles with a block co-polymer (poloxamine-908) suppresses opsonization but permits the activity of dysopsonins in the serum. Biochim Biophys Acta 1993;1179:157–165. [PubMed: 8218358]
51. Storm G, Belliot SO, Daemen T, Lasic DD. Surface Modification of Nanoparticles to Oppose Uptake by the Mononuclear Phagocyte System. Adv Drug Del Rev 1995;17:31–48.
52. Tan JS, Butterfield DE, Voycheck CL, Caldwell KD, Li JT. Surface modification of nanoparticles by PEO/PPO block copolymers to minimize interactions with blood components and prolong blood circulation in rats. Biomaterials 1993;14:823–833. [PubMed: 8218736]
53. Matsumura Y, Maeda H. A new concept for macromolecular therapeutics in cancer chemotherapy: mechanism of tumoritropic accumulation of proteins and the antitumor agent smancs. Cancer Res 1986;46:6387–6392. [PubMed: 2946403]
54. Gerlowski LE, Jain RK. Microvascular permeability of normal and neoplastic tissues. Microvasc Res 1986;31:288–305. [PubMed: 2423854]
55. Jordan A, Scholz R, Wust P, Fahling H, Felix R. Magnetic fluid hyperthermia (MFH): Cancer treatment with AC magnetic field induced excitation of biocompatible superparamagnetic nanoparticles. J Magn Magn Mater 1999;201:413–419.
56. Urano M, Kuroda M, Nishimura Y. For the clinical application of thermochemotherapy given at mild temperatures. Int J Hyperthermia 1999;15:79–107. [PubMed: 10323618]
57. Wust P, Hildebrandt B, Sreenivasa G, Rau B, Gellermann J, Riess H, et al. Hyperthermia in combined treatment of cancer. Lancet Oncol 2002;3:487–497. [PubMed: 12147435]

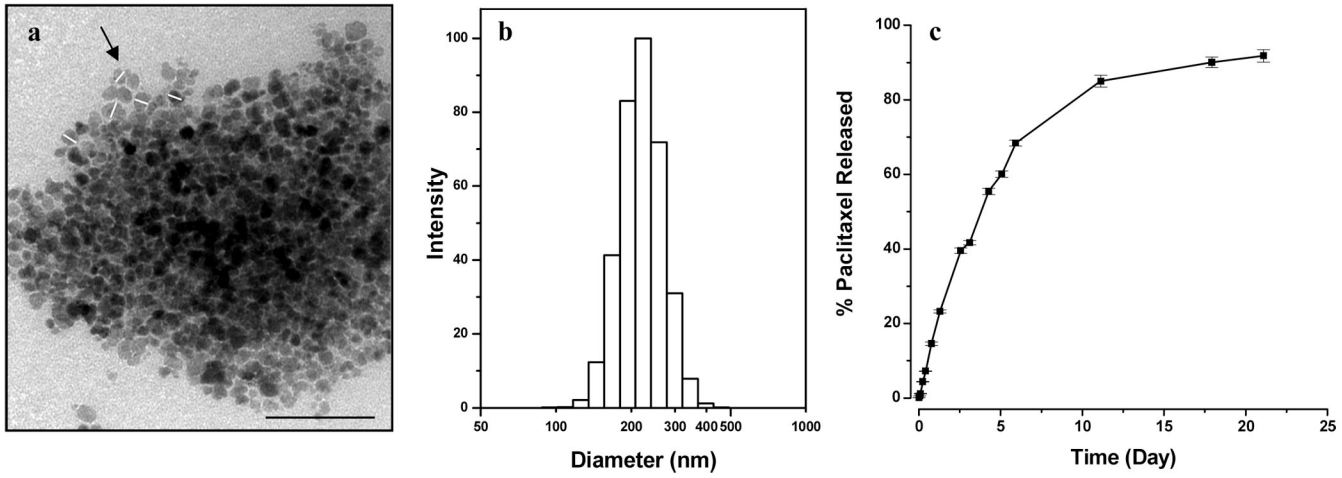

Figure 1.

Characterization of magnetic nanoparticles (MNPs). (a) Transmission electron micrograph of MNPs (Bar = 100 nm). White lines drawn across few particles (see black arrow) indicate the diameter of the iron-oxide core which was measured using ImageJ software, (b) Hydrodynamic particle size distribution of MNPs in water measured by using dynamic laser light scattering, and (c) Release of paclitaxel from MNPs under *in vitro* condition. The drug loading in MNPs was 9.5% w/w. Data as mean ± s.e.m. (n = 3).

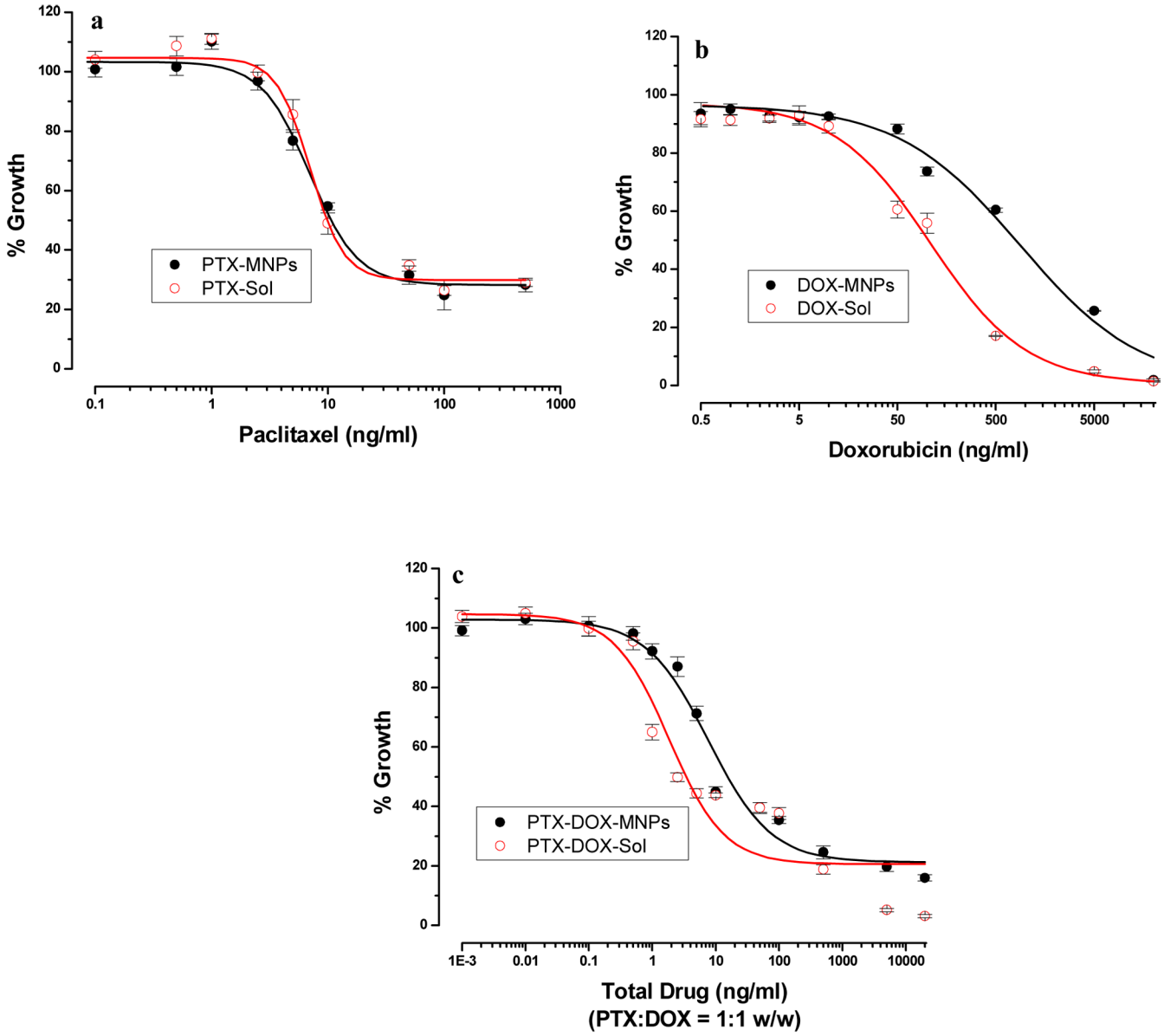

Figure 2.

Antiproliferative effect of drugs in solution and loaded in MNPs with (a) paclitaxel, (b) doxorubicin and (c) combination of paclitaxel and doxorubicin in MCF-7 cells. Cells were treated with drug either in solution or loaded in MNPs, medium was changed on day 2 and 4, and cell viability was measured using an MTS assay on day 5. Data as mean ± s.e.m. (n = 6).

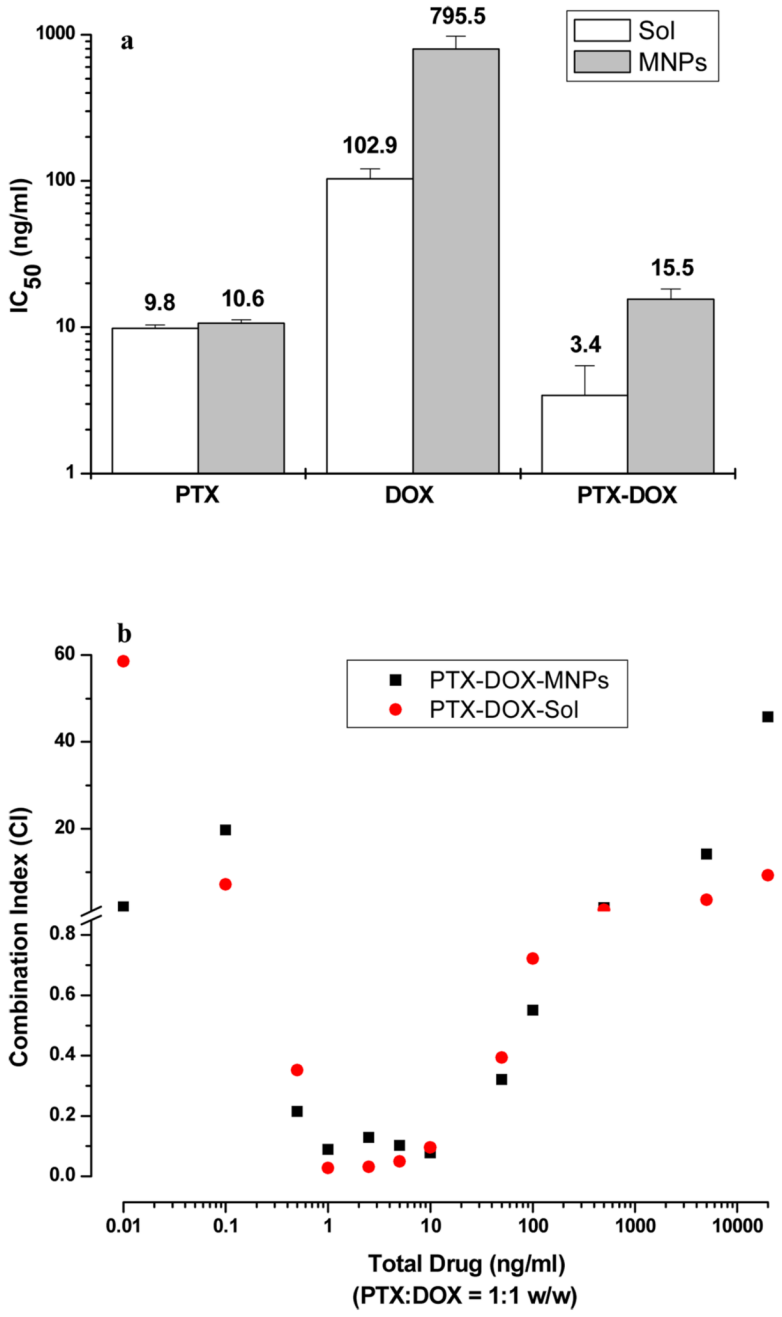

Figure 3.

Antiproliferative effect of drugs in MCF-7 cells. (a) IC_{50} values for paclitaxel, doxorubicin and combination of paclitaxel and doxorubicin (1:1 w/w ratio) in solution (white bar) and loaded in MNPs (gray bar). (b) The combination index values for the combination of drugs in solution or loaded in MNPs. Data as mean ± s.e.m. (n=6).

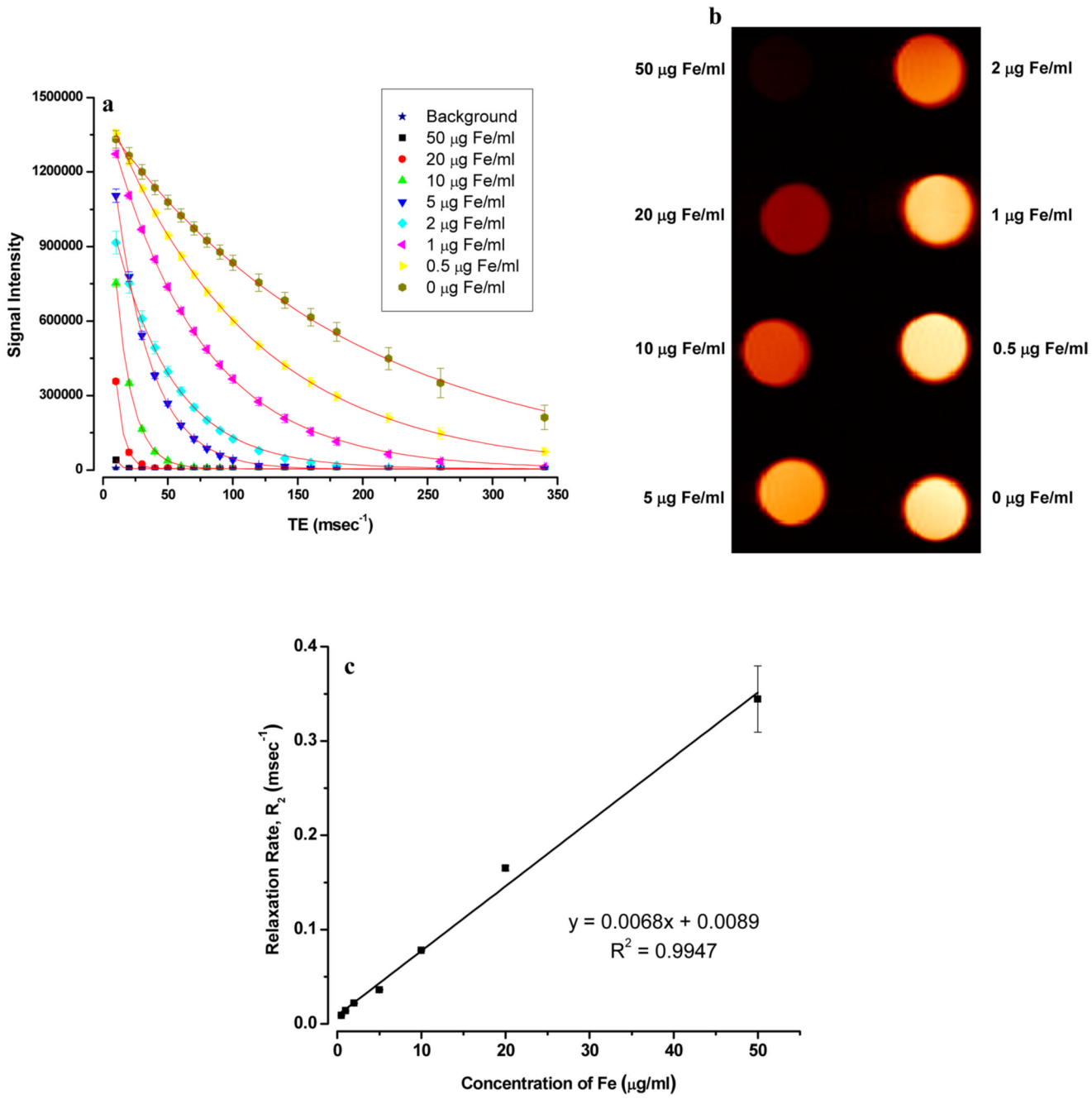

Figure 4.

Magnetic resonance imaging properties of MNPs. (a) T_2 relaxation analysis curves of MNPs in phantom agar gel at different iron concentrations (Data as mean intensity within ROI with standard deviation in intensities of pixels). (b) Signal intensity weighted images (TR = 10,000 msec, TE = 10 msec) of MNPs in phantom agar gel at various iron concentrations at 25 ° C, blank phantom agar gel was taken as a control. (c) T_2 relaxation rate (R_2) of MNPs versus iron concentration. (Data as values obtained from curve fitting and standard errors are uncertainties in fitting).

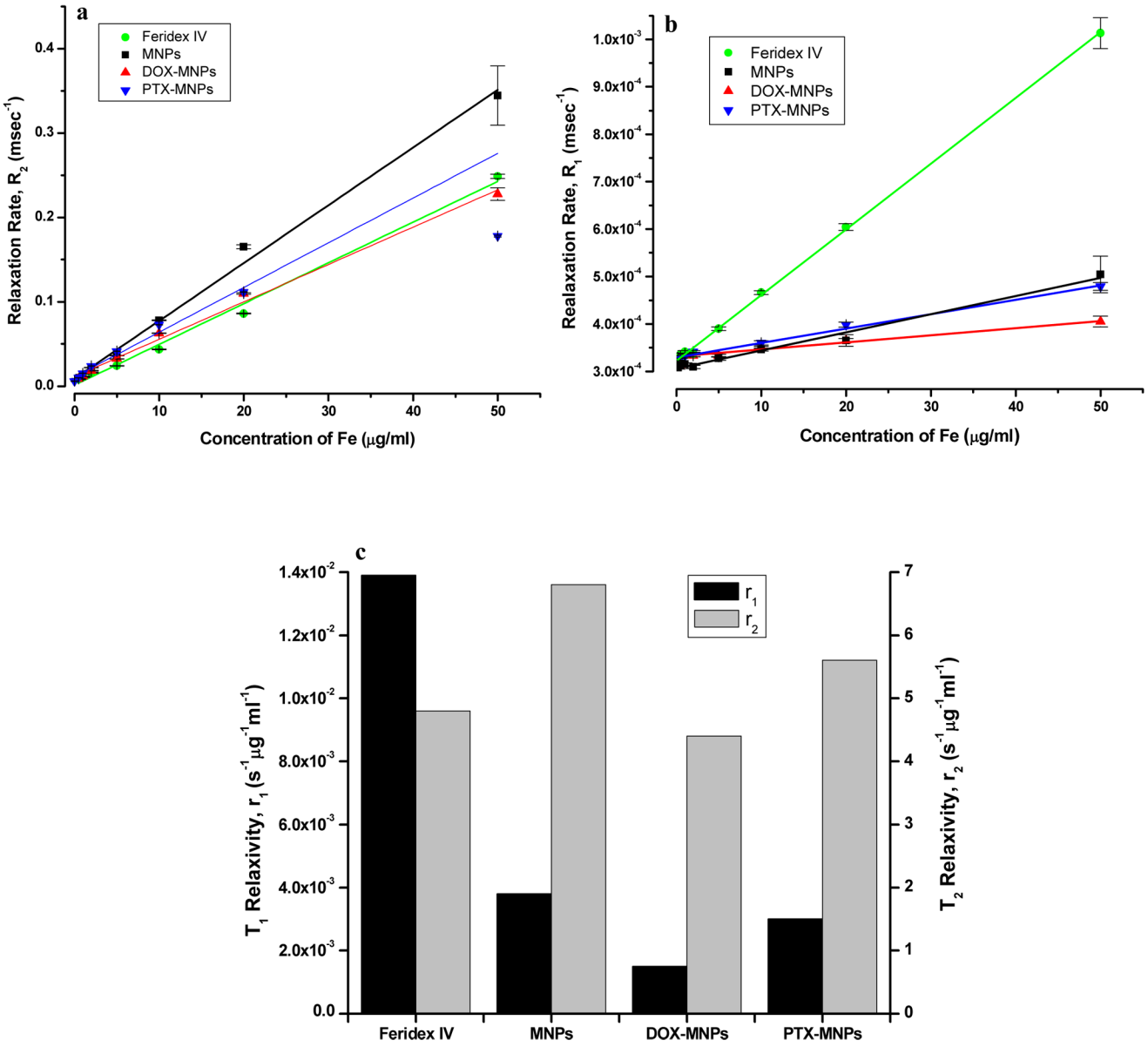

Figure 5.

Effect of loaded drugs on magnetic resonance imaging properties of MNPs. (a) T_2 relaxation rate (R_2), and (b) T_1 relaxation rate (R_1) of different formulations of MNPs with and without loaded drugs and Feridex IV at various iron concentrations. (c) Comparison of T_1 relaxivity (r_1) and T_2 relaxivity (r_2) of different formulations of MNPs. (Data as values obtained from curve fitting and standard errors are uncertainties in fitting).

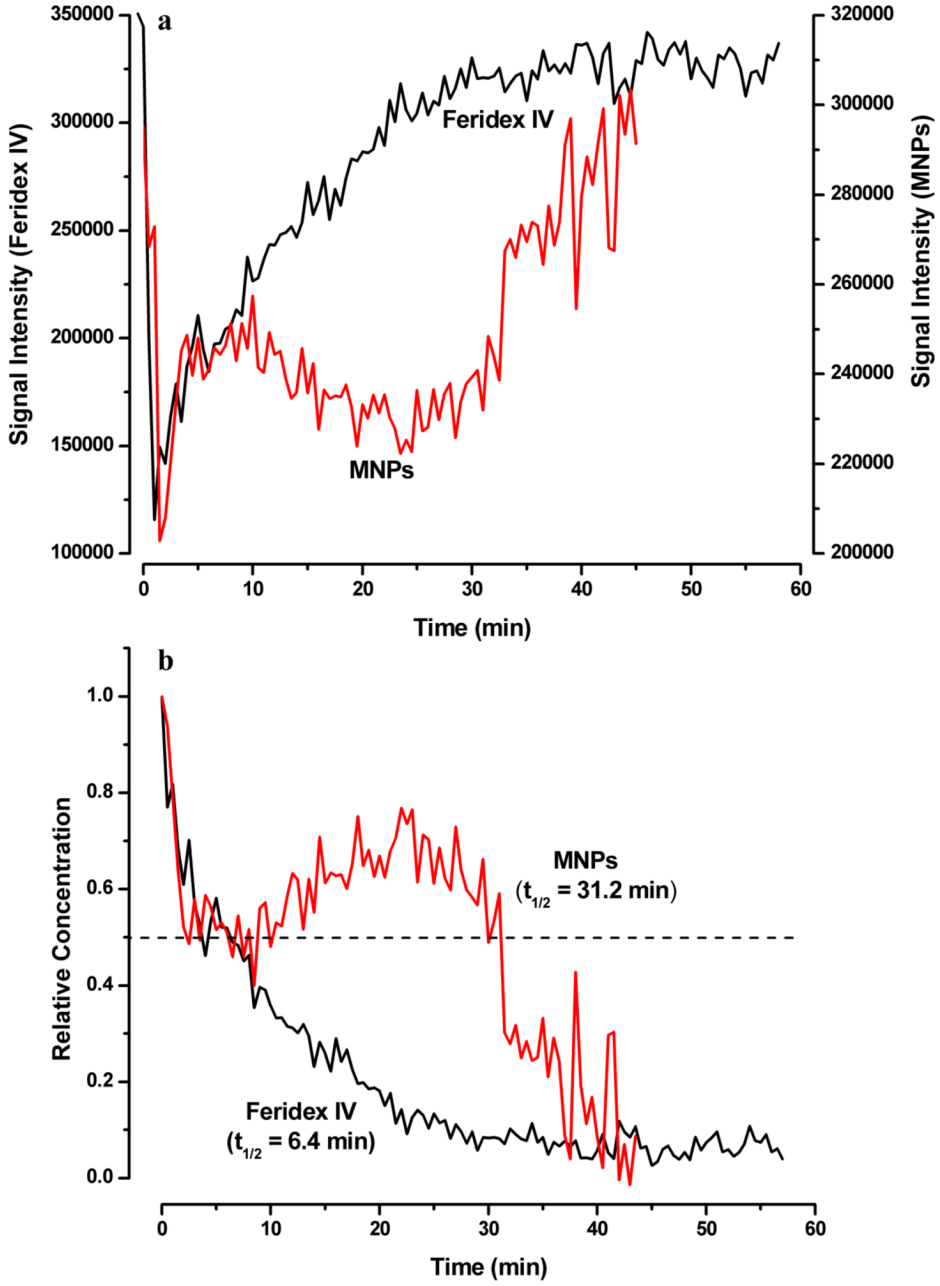

Figure 6.

Circulation half-life of magnetic nanoparticles in mice. (a) Changes in the MRI signal intensities measured in the ROIs of the carotid artery following intravenous injection of Feridex IV (Black) and MNPs (Red) to athymic nude mice at a dose of 7 mg Fe/kg. (b) Calculated relative iron-oxide concentration vs. time profiles in carotid artery for Feridex IV and MNPs. Half-life ($t_{1/2}$) of clearance of particles was read at the relative concentration = 0.5 (dashed line). Shown is the change in one carotid artery but both the carotid arteries showed almost identical pattern.

Table 1

Particle size and zeta potential of different formulations of MNPs.[a]

Sample	Water		PBS		Zeta (mV)	
	Diameter (nm)	PI	Diameter (nm)	PI	Water	PBS
Feridex IV	141.8±2.5	0.285±0.008	138.0±0.9	0.288±0.006	−31.30±0.82	0.69±0.25
MNPs	222.4±2.5	0.080±0.013	211.3±3.5	0.237±0.034	−31.91±2.10	2.22±0.30
DOX-MNPs	213.5±2.5	0.050±0.020	240.8±1.9	0.037±0.008	−10.10±0.54	0.07±0.33
PTX-MNPs	248.4±2.1	0.105±0.007	246.3±4.6	0.048±0.024	−29.25±0.92	1.98±0.36

[a] Data as mean ± s.e.m. (n=3)

Table 2

Saturation magnetization measurements of MNPs in phantom agar gels at different iron concentrations.[a]

Gel	Ms (emu/ml of gel)		
	2 mg Fe/ml	1 mg Fe/ml	0.5 mg Fe/ml
Feridex IV	0.168	0.070	0.040
MNPs	0.321	0.091	0.060
DOX-MNPs	0.203	0.093	0.042
PTX-MNPs	0.262	0.117	0.058

[a] Data as values obtained from curve fitting. Samples were measured once and uncertainty in the fitting was determined.

Table 3

Drug loading of doxorubicin and paclitaxel in MNPs.[a]

Doxorubicin		Paclitaxel		Total Drug Loading (% w/w)
Added (% w/w)	Loaded (% w/w)	Added (% w/w)	Loaded (% w/w)	
0.0	0.0	10.0	9.5 ± 0.2	9.5 ± 0.2
5.0	3.7 ± 0.2	5.0	4.8 ± 0.1	8.5 ± 0.1
10.0	8.2 ± 0.3	0.0	0.0	8.2 ± 0.3

[a] Data as mean ± s.e.m. (n=3)

Table 4

T_1 and T_2 relaxivities of different formulations of MNPs in phantom agar gels.

Sample	T_1 relaxivity (r_1) ($s^{-1}\mu g^{-1}ml$)	T_2 relaxivity (r_2) ($s^{-1}\mu g^{-1}ml$)
Feridex IV	13.9×10^{-3}	4.8
MNPs	3.8×10^{-3}	6.8
DOX-MNPs	1.5×10^{-3}	4.4
PTX-MNPs	3.0×10^{-3}	5.3